Surface free energy analysis of electrospun fibers based on Rayleigh-Plateau/Weber instabilities

Urszula Stachewicz[1,2,3], J. Frits Dijksman[4], Chaïma Soudani[2], Lewis B. Tunnicliffe[2], James J. C. Busfield[2] and Asa H. Barber[1,2,5]*

[1]Nanoforce Technology Ltd., Queen Mary University of London, Mile End Road, London E1 4NS, United Kingdom

[2]School of Engineering and Materials Science, Queen Mary University of London, Mile End Road, London E1 4NS, United Kingdom

[3]AGH University of Science and Technology, International Centre of Electron Microscopy for Materials Science and Faculty of Metals Engineering and Industrial Computer Science, Al. A. Mickiewicza 30, 30-059 Kraków, Poland

[4]University of Twente, Faculty Science and Technology, Physics of Fluids, Drienerlolaan 5, 7522NB Enschede, The Netherlands

[5]School of Engineering, University of Portsmouth, Portsmouth PO1 3DJ, United Kingdom

*CORRESPONDING AUTHOR EMAIL ADDRESS: ustachew@agh.edu.pl

Abstract

Electrospinning is an increasingly common technique used to produce fibers with a range of diameters. These electrospun fibers are used extensively in applications that exploit the material's high surface area to volume ratio, thus requiring detailed knowledge of the surface properties of the fibers. The surface free energy of individual free standing electrospun styrene-butadiene rubber (SBR) fibers was determined here from the time-dependent break-up of long fibers driven initially by Rayleigh-Plateau/Weber instabilities. Individual free standing electrospun rubber fibers were observed to change from a cylindrical fibrous geometry to semi-spherical droplets during a time period of several days when above the glass transition temperature of the polymer. A wave-like transition from fiber to droplet was attributed to a surface tension driven break-up process occurring over a time strongly influenced by the rubber's viscosity. The surface free energy for an electrospun rubber fiber was found using a Weber approach for the free standing fibers and Diez et al theory for dynamic fluid instability of fluid ridges. Both methods lead to similar values of fiber surface free energy and were confirmed from bulk measurements exploiting Owens-Wend theory. The approach presented here is powerful as the surface free energy, indicative of the physical and chemical behavior of the fiber surface, can be determined for any fiber diameter provided the geometric break-up of the fiber is observed.

Keywords

Surface free energy, Rayleigh-Plateau/Weber instabilities, Fibers, Rubber, Electrospinning, Fluids

1. Introduction

Electrospun polymer fibers are used extensively for applications where their large ratio of surface area and volume is of critical importance, such as for filtration,[1] tissue engineering,[2-3] energy[4] and in composites[5-6]. Electrospun fibers have benefits over many other fibrous materials due to their relatively large surface area to volume ratio, especially when fiber diameters approach nanoscale dimensions. The physical and chemical properties of the fiber surface, in addition to geometric considerations, define electrospun fiber performance.[7-8] Recent work has highlighted how the physical properties of electrospun polymer fiber surfaces, quantified by the surface free energy, differ from bulk polymer behavior[9] using a modified Wilhelmy balance approach applied to individual fibers[10]. While this work is powerful in measuring electrospun fiber surface free energy, a number of complex nano-manipulation steps are required prior to testing.[11] This paper seeks to define a method of measuring the surface free energy of electrospun polymer fibers by using surface energy driven polymer flow generally described by Rayleigh-Plateau/Weber instability.[12-14] Rayleigh-Plateau/Weber instabilities are notable in the electrospinning process when a polymer solution in the form of a jet is drawn under the action of an electric field.[15] During electrospinning, the typically rapid solvent evaporation, which reduces polymer chain mobility until solid polymer is collected, competes against the surface energy driven instability and break-up into droplets. Similar instabilities were observed recently[18] when annealing nanowires at 400-600 ºC [19] as well as during ink-jet printing[20] and electrospraying processes for aerosols of liquid and solid particles.[21-26] For fibrous geometries, the surface of the cylindrical shape is always initially perturbed if material is able to flow. This perturbation is manifest as the formation of initial crests and troughs of specific wavelength in fiber topography that initiate the break-up process. The fiber curvature drives material to flow from the troughs to the crests, amplifying the wave amplitude, and this arises when the polymer molecules have sufficient mobility. The Rayleigh-Plateau/Weber wavelength is defined for the break-up process that proceeds at the highest rate. Such a break-up process can be avoided by using liquid phases with low mobility, as used when electrospinning high viscosity polymer solutions to produce nanofibers, or accelerated with a higher mobility phase. Rubber materials are an

example of a polymer where cross-linking between the polymer chains is used to reduce their mobility. Conversely, a rubber material prepared without cross-linking will exhibit viscous characteristics and flow with time as the polymer macromolecular chains are able to move away from the troughs to initiate break-up. Observing rubber material above its glass transition temperature provides sufficient mobility for polymer chains to break-up the fibrous geometry into droplets. The uncross-linked rubber behaves as a viscous fluid above its glass transition temperature and is therefore considered as such when developing methods to evaluate the surface free energy contribution to this process. As Rayleigh-Plateau/Weber instability is driven by surface free energy, observing break-up of fibers of such non-cross-linked rubbery polymers can provide information on the surface free energy when the viscosity of the material is known. Previous work has shown how surface free energy values of fluid systems can be estimated from recording geometric changes.[27] Therefore, the surface free energy of fibers using Rayleigh-Plateau/Weber instability principles can be calculated by observing the break-up of electrospun rubber fibers driven by their surface free energy and by measuring the relaxation times involved in the process. Efforts to describe the flow of polymer were developed from initial perturbation of cylindrical geometries using Rayleigh-Plateau/Weber,[13-14] through Diez et al.[32] and finally more established surface free energy method measured at equilibrium using the common contact angle measurement approach and interpretation using Owens-Wendt theory.[33] We use these Rayleigh-Plateau/Weber and Diez et al. theories to calculate the surface free energy from fiber break-up. The Rayleigh-Plateau/Weber mechanism is applied for the initially cylindrical shape of electrospun fibers. In this study we observe a styrene-butadiene rubber (SBR) without cross-links that acts as a viscoelastic polymer liquid and attempt to understand the mechanism of expected break-up of the fibers into droplets.

2. Materials and Methods

2.1. Electrospinning of rubber fibers

Rubber nanofibers were prepared using electrospinning. Styrene-butadiene rubber (SBR, Emulsion, Europrene 1502, Polimeri Europa, U.K.) with an weight average molecular weight (M_w) of 686346 g.mol^{-1}. Molecular weight was determined by gel permeation chromatography using an Agilent 1260 GPC. Tetrahydrofuran/2% triethylamine eluent without any cross-linkers was first dissolved in a mixture of tetrahydrofuran (THF, AnalaR NORMADUR, VWR BDH Prolabo, U.K.) and dimethylformamide (DMF, 99.8%, Sigma Aldrich, U.S.A.) (75/25 % mass ratio) to produce a polymer concentration of 5 wt. % in solution. The SBR solution was electrospun from a pin electrode using commercially available equipment (Nanospider, Elmarco, Czech Republic). A voltage of 26 kV was applied between the pin electrode situated 16 cm above a ground electrode. Experiments were performed at room temperature (21-22 ˚C) and a humidity of 30-36%.

2.2. Optical microscopy observations

Electrospun SBR fibers were deposited onto glass slides to allow subsequent observation of the fiber geometry using optical microscopy (Olympus BX 60 with Digital Imaging, Japan), as shown in Figure 1. The microscope light was used for short observation times of 5 s to avoid any heating of the rubber fibers from the light source. We assumed that the electrospun SBR fibers are loosely distributed over the substrate surface after electrospinning and contact the substrate at a limited number of points. Fiber dimensions were measured from optical images using Image J (version 1.48v, National Institutes of Health, U.S.A.). The free standing cylindrical geometry of the SBR fibers was observed to attach to the substrate and break-up into droplets over a period of 6 days. The break-up time was defined from the total time measured from the point of fiber deposition onto the glass slide. The break-up phenomena of 6 different fibers, shown in Figure 1, with initial diameters ranging from 1 to 2.2 μm, at 5 random points along the fiber length were measured optically over 6 days. Fiber irregularity observed during Rayleigh-

Plateau/Weber break-up, as shown in Figure 2, is due to perturbation growth observed in the form of crests and troughs.

2.3. Viscosity measurement

The viscosity of SBR in liquid form was determined within the low-shear Newtonian plateau at room temperature from tensile creep experiments on molded cylindrical samples. Extensional viscosity was calculated from the applied tensile stress divided by the strain rate at steady state creep and converted to shear viscosity via the Trouton ratio, giving an average SBR viscosity of 281.8 MPa · s.[34] Cross-linked SBR has a modulus of 1 – 4 MPa.[35-36]

2.4. Surface free energy calculations and measurements

Uncross-linked rubbers act as viscoelastic liquids so that free standing fibers with an initial non-equilibrium cylindrical shape tend to break-up into droplets. This geometric change is driven by surface tension to minimize surface area. The initial Rayleigh-Plateau/Weber state occurs when the cylindrical shape of the electrospun fibers is perturbed within the first day of optical observations (Figure 2(a)). After the first day, fibers attach to the surface of the substrate and form fluid ridges (rivulets). The break-up of these rubber rivulets can be understood by applying the theory described by Diez et al, which includes the contact angle between rubber materials and substrate. The break-up time is the total time measured from the beginning of the experiment, which was continued up to 6 days. Notable, on the time scale of the experiment the fluid behaves totally Newtonian and the stress relaxation in fibers takes place at a short time compared to the timing of the experiment. The optical microscopy images of rubber fibers were taken and the cross-sectional dimensions of fibers determined.

Surface free energy calculations were carried out by assuming the entanglement density of uncross-linked SBR were comparable to the cross-link density of standard cross-linked SBR. This statement can be justified by the fact that free volume of non-cross-linked and cross-linked SBR is similar, suggesting a constant number density of contact points between the polymer chains. Upon cross-linking, these

contact points become chemical bonds, whereas in uncross-linked rubber these contact points are temporary entanglements. The ratio of the viscosity and the elastic modulus of the SBR define a time constant during which viscoelastic effects are present. This ratio in our experiments shown below is about 100-500 s, which is relatively small compared to the number of days considered in the experiment, indicating that viscoelastic effects can be ignored.[37] The organization of the polymer chains progress from an initial aligned condition to a relaxed random orientation. For the fastest growing mode of a Rayleigh-Plateau/Weber instability of a free liquid fiber including the effect of viscosity, Weber derived an equation to calculate the break-up time thus: [14,38]

$$\tau = \left(\sqrt{\frac{8\rho R_1^3}{\gamma}} + 6\frac{\eta R_1}{\gamma} \right) \ln \frac{R_1}{\delta^*} \qquad (1)$$

where τ is the break-up time, ρ is the density of SBR, γ is the surface tension of SBR, R_1 is radius of the undisturbed mobile fiber of η viscosity and δ^* initial disturbance. In principle a perfect cylindrical tube does not collapse into separate droplets and this process must be set in motion by an initial disturbance distance of the cylindrical shape, indicated by δ^*. Larger disturbances cause faster fiber decomposition into droplets. As the viscosity is initially high for the electrospun fiber, the first term $\sqrt{\frac{8\rho R_1^3}{\gamma}}$ in equation (1) can be neglected. The optimal wavelength at which the instability grows fastest increases with increasing viscosity. The break-up phenomenon for fibers of limited length, but long compared to their cross-sectional dimensions, is therefore localized. Break-up occurs irregularly and no communication along the fiber as far as the onset of instabilities occurs. Electrospun rubber nanofibers have initial cross-sectional deviations over their length as large as 20%. Equation (1) describes the time taken for the fiber to break up given an initial disturbance. Measuring the break-up time for a fiber with radius R_1 and 20% diameter variations provides an expression for the interfacial tension that is derived as:

$$\gamma = 10\frac{\eta R_1}{\tau} \tag{2}$$

Equation (2) provides a means for the calculation of the surface free energy for the initial free standing cylindrical fiber shape and does not hold for a general non-cylindrical geometry. Despite electrospun fibers contacting the glass slide surface, the Weber theory can be applied as the instability is more a localized phenomenon rather than a continuous distribution of wave along the fiber where substrate interactions can dictate.

After some time the fiber comes in contact with and starts to wet the substrate. The initial circular cylindrical shape makes a transition to a fluid ridge. Such a fluid ridge can be considered as a cut-off from a circular cylinder with radius R_2. Progression of the fiber relaxation from a cylindrical geometry to a fluid ridge through a break-up transition requires application of the Diez et al. theory: [39-41]

$$\gamma = 160\frac{\eta R_2}{\tau}\frac{\sin\theta}{\theta^3}, \tag{3}$$

where R_2 is the initial radius of curvature of a straight ridge and θ is the contact angle between the rubber, behaving as a viscous fluid, and substrate. The relation between the width w, the radius of curvature R_2 of the cross-section of the fluid ridge and the contact angle θ is given by:

$$w = 2R_2\sin\theta \tag{4}$$

As no material is lost during the experiment, the radius of curvature of the fluid ridge R_2 is related to the original fiber radius R_1 through:

$$\pi R_1^2 = R_2^2\left(2\theta - \sin 2\theta\right) \tag{5}$$

Equations (4) and (5) allow for the calculation of R_2 and θ by measuring the width of the fluid ridge and the initial fiber radius. Extended time periods over several days cause an increase in the width of the fluid ridge such that the contact angle calculated with equations (4) and (5) becomes smaller than unity,

limiting the use of Diez et al. equation only for the later stages of the break-up. We assume, however, that the Diez formula applies for the whole process of the break-up of the spreading fluid ridge. Comparing equations (3) and (2) indicates that the break-up time of a fluid ridge is much larger than the break-up time of a free fiber, and small values of the contact angle provide infinite break-up times.

5. Contact angle measurement on a rubber film

SBR films were prepared to provide macroscopic surface free energy comparisons to electrospun SBR fibers. A structurally isotropic SBR film is expected to have a comparable surface free energy to a structurally isotropic electrospun fiber. The SBR films were produced by placing approximately 2 ml of the SBR solution used for the electrospinning onto a glass slide rotating at 2000 rpm for 1 min in a spin coating (SCS G3 Spin Coater, U.S.A.). The thickness of the resultant dry SBR film on the glass slide was 0.4±0.1 mm as confirmed using a micrometer. The surface free energy of the SBR film was found using contact angle measurements. Specifically, droplets of polyethylene glycol, glycerol and deionized water were deposited onto the SBR films and resultant contact angles measured using a Drop Shape Analysis System (Krüss, DSA100, Germany) as shown (Figure 3 (a) and Table I). The error bars on the measured contact angles were determined based on standard deviation calculations.

The surface free energy of the comparison SBR films was quantified using Owens-Wendt theory[33] to determine the polar and dispersive contributions to a film's surface free energy using the known polar and dispersive components of the probe liquids and their contact angles with the solid film using equation (6) below:

$$\frac{\gamma_l\left(1+\cos\theta_{film}\right)}{2\sqrt{\gamma_l^d}}=\sqrt{\gamma_s^p}\left(\frac{\sqrt{\gamma_l^p}}{\sqrt{\gamma_l^d}}\right)+\sqrt{\gamma_s^d} \qquad (6)$$

where γ_l is the total surface tension of the liquid with dispersive γ_l^d and polar γ_l^p components and γ_s is the surface free energy of a solid film surface with dispersive γ_s^d and polar γ_s^p components. θ_{film} is the contact angle made between the probe liquid and solid SBR film surface as measured using the Drop Shape Analysis System. An Owens-Wendt plot is formed from Eq. (6) from a simple linear function of $y = mx+b$, where the axis terms of $y = \frac{\gamma_l(1+\cos\theta_{film})}{2\sqrt{\gamma_l^d}}$ and $x = \frac{\sqrt{\gamma_l^p}}{\sqrt{\gamma_l^d}}$ are known using the data presented in Table I. Thus, a linear plot of these two terms for each probe liquid wetting the SBR film surface can be used to determine the polar and dispersive components of the solid surfaces where $m = \sqrt{\gamma_s^p}$ and $b = \sqrt{\gamma_s^d}$ as shown in Figure 3(b). The sum of polar (24.4 mJm^{-2}) and dispersive (14.4 mJm^{-2}) components gives the total solid surface free energy of SBR films, resulting in a total SBR surface free energy of 38.8 (SD=1.0) mJm^{-2}.

3. Results and Discussion

The break-up of electrospun SBR fibers was observed using optical microscopy over 6 days as shown in Figure 2. The break-up is characterized by an initially rapid loss of the fibrous geometry over approximately 12 hours governed by the Rayleigh-Plateau/Weber instabilities presented in Figure 2(a), followed by a slower break-up and finally a flow phenomenon that ends up in separate droplets of rubber on the surface of the substrate, Figure 2 (b-d). The fastest growing mode determines the growth rate of the disturbance and the break-up time. However, progression of the break-up causes the free fiber to contact with and spread over the surface of the substrate. The ridge of viscoelastic polymer liquid slowly grows in width and finally breaks up into droplets of mobile rubber. From the optical microscopy observation, the diameter of fiber and width of the ridge were measured at the onset of fiber break-up after 2 days. The obtained data were used to calculate surface free energy using equations (2) and (3) for the initial and break-up point respectively. For the former, the surface free energy of SBR fibers, γ_f, was

calculated from observations over the initial 12 hour period and applying the Rayleigh-Plateau/Weber[14] equation (2).

The surface free energy values for fibers within the first 12 hours obtained from Weber's equation is 46.7 (SD=14.4) mJm^{-2}. The increase of surface free energy of rubber fibers comparing to film is roughly 20%, and is similar to observations for nylon 6 electrospun nanofibers compared to the corresponding film.[9] The Diez et al. theory in equation (3) was applied to observations from 2 to 4 days and resulted in a surface free energy from 41.7 (SD=15.5) mJm^{-2} to 32.8 (SD=13.5) mJm^{-2} during this time period. The surface free energy values with time for a range of fiber diameters are shown in Table II and suggest a consistency, within error, of surface free energy measurements when considering theories suitable for the mechanistic changes in fluid flow. These results need to be additionally compared to literature that considered structural orientation in electrospun fibers. Our previous work suggested an increase in surface free energy due to increase order (polymer chains alignment) in polymer fiber structure[9] and film[42]. The alignment of polymer chains during electrospinning and collecting fibers on a rotating drum, with mechanical drawing of fibers, causes fiber elongation and an increase of Young's modulus.[29,31]. The increase of surface free energy by changing the internal energy and entropy of the bulk polymer material, for example by stretching the sample and aligning polymer chains, increases surface free energy.[43] The polymer chains at the surface of electrospun fibers are therefore known to be aligned along the principle fiber length.[28] The loss of the alignment occurs due to polymer chain mobility and relaxation, indicating that the surface free energy of electrospun fibers should initially be relatively high and drop due to relaxation to an isotropic state. This relaxation of polymer chains should occur quickly after the deposition of SBR fibers so that resultant surface free energy reaches a constant value with time as the polymer chain lose alignment and behave as the bulk surface. The use of SBR above the glass transition temperature in this work relaxes rapidly after the electrospinning step so that all surface free energy measurements can be considered to be at a constant value for a relaxed isotropic structure. The surface free energy calculations for the fibers both initially and during break-up are compared to the

bulk film, established with the Owens-Wendt method as presented in Figure 3 and Table I, shown in Figure 4. The fiber surface free energy shows a relatively consistent value over a period of 6 days in Figure 4 and is comparable to the bulk SBR measurements. The lack of a potential drop in surface free energy to a constant value with time for the fibers and the similarity to the bulk SBR film calculations strongly suggests that the electrospun fibers are indeed in a relaxed isotropic state. The use of the two distinct Rayleigh-Plateau/Weber and Diez et al. theories are also consistent in providing comparable surface free energy values for the electrospun SBR fibers. Mechanistic changes in the temporal evolution of droplets from fibers are thus fully described in this work. We note that the standard deviation in the calculated surface free energy values in Figure 4 are 15 mJm^{-2}, which is too great to determine any variation in surface free energy due to fiber diameter. We would not expect physical properties to change above diameters of 1 micron and typical size effects in electrospun fibers are encountered at sub-micron dimensions.[11,28-29] However, improved observational accuracy providing potentially smaller calculated surface free energy error is expected when using a higher spatial resolution microscope, such as electron microscopy, as opposed to the optical evaluations of this work.

4. Conclusions

To conclude, we have demonstrated the use of Rayleigh-Plateau/Weber instabilities of a fiber and Diez et al. theory of the instability of a fluid ridge on a flat substrate to quantify the surface free energy of electrospun fibers of SBR, which are comparable to macroscopic surface free energy measurements of bulk SBR films. While this work has evaluated fibers with diameters of the order of 1-2 microns, the approach may be applied to smaller diameter polymer fibers provided the microscopy is of sufficient resolution to elucidate the break-up process and the polymer is sufficiently mobile.

Acknowledgments

The authors thank Dr Zofia Luklinska at Queen Mary University of London NanoVision Centre for assisting with the microscopy facilities.

FIGURES

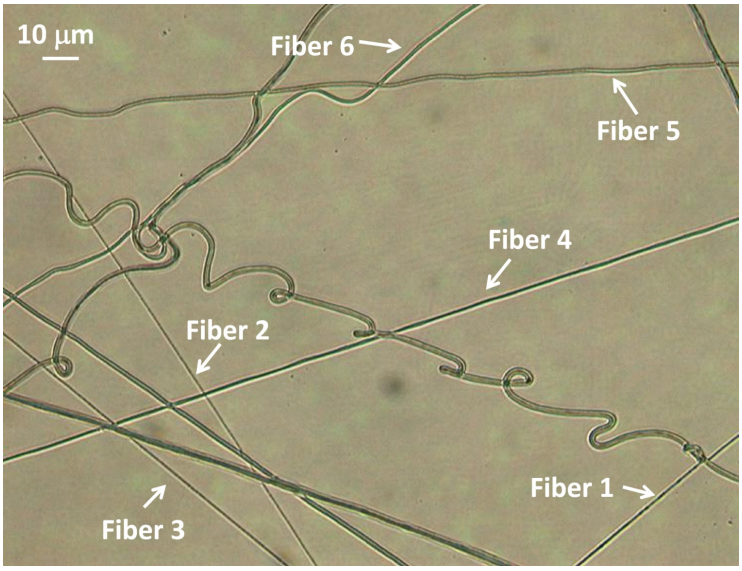

Figure 1. Optical micrographs showing electrospun rubber fibers used for surface free energy analysis.

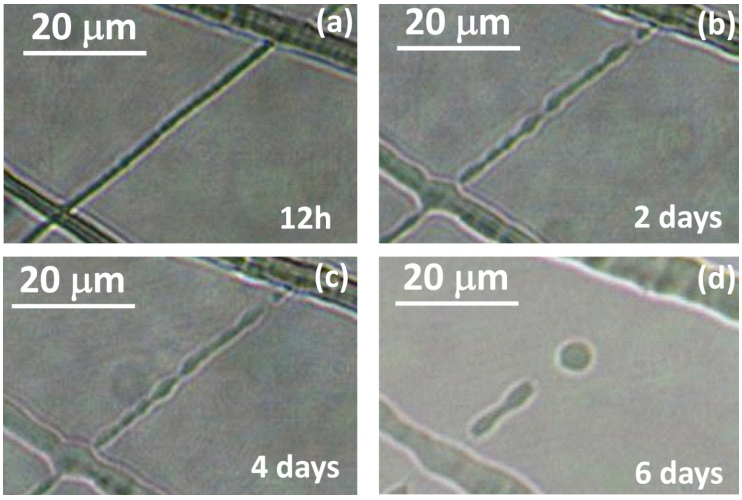

Figure 2. Optical micrographs of break-up process of electrospun SBR fiber 1 (shown in Figure 1) over a 6 day period. (a) During the 12 hour experiment it is supposed that the fiber is free standing. (b-c) For the later experiments the fibers adheres to the substrate and starts spreading and become more and more unstable. (d) After break-up the fluid collects into pools of liquid (after 6 days).

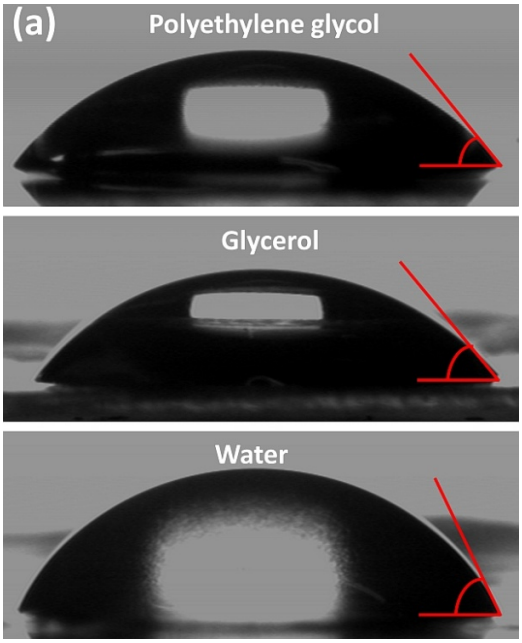

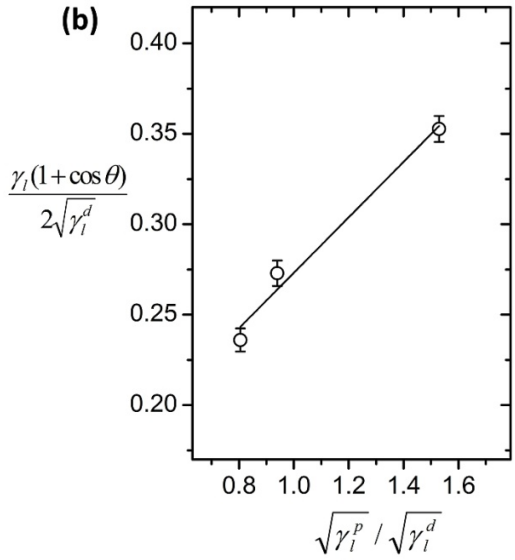

Figure 3. (a) Optical micrographs of polyethylene glycol, glycerol and deionized water droplet contact angles on SBR films. Note the smallest contact angle is achieved for the lowest surface tension liquid of polyethylene glycol on the SBR film whereas the largest contact angle is found for the highest liquid surface tension of water. The average of the measured contact angles are presented in Table I. (b) Owens-Wendt plot for the three probe liquids of differing surface tension wetting the SBR film surface.

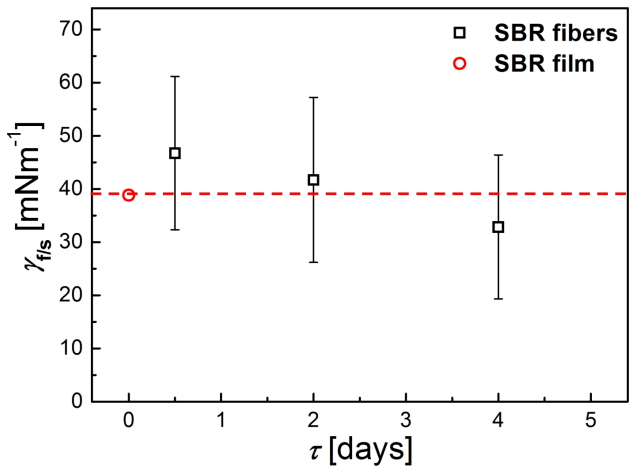

Figure 4. Plot of the surface free energy values of electrospun SBR fibers, calculated based on the Rayleigh instabilities observations using Rayleigh-Plateau/Weber theory of equation (1) for 0.5 day and Diaz et. al. theory with Equation (3) for 2 and 4 days, with time and the corresponding surface free energy of SBR film, indicated with dashed line.

TABLES:

TABLE I. Surface tension data for three probe liquids used for wetting experiments in Figure 3, stating the total surface tension, γ_l, the dispersive, γ_l^d, and polar, γ_l^p, components from [9,42,44-45] The corresponding contact angle measurements are given for each probe liquid on SBR films.

Liquid	γ_l [mJm^{-2}]	γ_l^d [mJm^{-2}]	γ_l^p [mJm^{-2}]	θ [°]
Polyethylene glycol	48.3	29.4	19.0	47.7 ± 1.3
Glycerol	64.0	34.0	30.0	55.0 ± 1.4
Water	72.8	21.8	51.0	64.5 ± 1.3

Table II. Surface free energy values for electrospun SBR fibers, obtained for the 12 hour data using Weber's equation (2), and for the 2 and 4 days experiments using Diez et al. equation (3)

Fiber number	Fiber diameter [μm]	Surface free energy [mJm^{-2}]		
		Time		
		12 h	2 days	4 days
1	1.27	41.4	45.8	34.4
2	1.08	32.5	21.5	17.3
3	1.02	30.7	24.5	20.9
4	1.94	58.4	44.4	29.0
5	2.21	66.6	55.8	42.0
6	1.69	50.9	58.3	53.5
Average		46.7	41.7	32.8
Standard deviation		14.4	15.5	13.5

References

1. Barhate, R. S.; Sundarrajan, S.; Pliszka, D.; Ramakrishna, S. Fine Chemical Processing: The Potential of Nanofibres in Filtration. *Filtr. Sep.* **2008**, 45, 32-35.
2. Venugopal, J.; Ramakrishna, S. Applications of Polymer Nanofibers in Biomedicine and Biotechnology. *Appl. Biochem. Biotech.* **2005**, 125, 147-157.
3. Stachewicz, U.; Qiao, T.; Rawlinson, S. C. F.; Almeida, F. V.; Li, W.-Q.; Cattell, M.; Barber, A. H. 3d Imaging of Cell Interactions with Electrospun Plga Nanofiber Membranes for Bone Regeneration. *Acta Biomater* **2015**, 27, 88-100.
4. Zhang, P.; Zhao, X.; Zhang, X.; Lai, Y.; Wang, X.; Li, J.; Wei, G.; Su, Z. Electrospun Doping of Carbon Nanotubes and Platinum Nanoparticles into the Beta-Phase Polyvinylidene Difluoride Nanofibrous Membrane for Biosensor and Catalysis Applications. *ACS Appl. Mater. Interfaces* **2014**, 6, 7563-7571.
5. Rein, D. M.; Cohen, Y.; Lipp, J.; Zussman, E. Elaboration of Ultra-High Molecular Weight Polyethylene/Carbon Nanotubes Electrospun Composite Fibers. *Macromol. Mater. Eng.* **2010**, 295, 1003-1008.
6. Stachewicz, U.; Modaresifar, F.; Bailey, R. J.; Peijs, T.; Barber, A. H. Manufacture of Void-Free Electrospun Polymer Nanofiber Composites with Optimized Mechanical Properties. *ACS Appl. Mater. Interfaces* **2012**, 4, 2577–2582.
7. Stachewicz, U.; Hang, F.; Barber, A. H. Adhesion Anisotropy between Contacting Electrospun Fibers. *Langmuir* **2014**, 30, 6819-25.
8. Stachewicz, U.; Peker, I.; Tu, W.; Barber, A. H. Stress Delocalization in Crack Tolerant Electrospun Nanofiber Networks. *ACS Appl. Mater. Interfaces* **2011**, 3, 1991-1996.
9. Stachewicz, U.; Barber, A. H. Enhanced Wetting Behavior at Electrospun Polyamide Nanofiber Surfaces. *Langmuir* **2011**, 27, 3024-3029.
10. Stachewicz, U.; Stone, C. A.; Willis, C. R.; Barber, A. H. Charge Assisted Tailoring of Chemical Functionality at Electrospun Nanofiber Surfaces. *J. Mater. Chem.* **2012**, 22, 22935-22941.
11. Hang, F.; Lu, D.; Bailey, R. J.; Jimenez-Palomar, I.; Stachewicz, U.; Cortes-Ballesteros, B.; Davies, M.; Zech, M.; Boedefeld, C.; Barber, A. H. In Situ Tensile Testing of Nanofibers by Combining Atomic Force Microscopy and Scanning Electron Microscopy. *Nanotechnology* **2011**, 22, 365708-8.
12. de Gennes, P.-G.; Brochard-Wyart, F.; Quere, D. *Capillary and Wetting Phenomena: Drops, Bubbles, Pearls, Waves*; Springer: New York, 2002.
13. Rayleigh, L. On the Capillary Phenomena of Jets. *P. R. Soc. London* **1879**, 29, 71-97.
14. Weber, C. Zum Zerfall Eines Flüssigkeitsstrahles. *ZAMM - Journal of Applied Mathematics and Mechanics / Zeitschrift für Angewandte Mathematik und Mechanik* **1931**, 11, 136-154.
15. Shin, Y. M.; Hohman, M. M.; Brenner, M. P.; Rutledge, G. C. Electrospinning: A Whipping Fluid Jet Generates Submicron Polymer Fibers. *Appl. Phys. Lett.* **2001**, 78, 1149-1151.
16. Luo, C. J.; Edirisinghe, M. Core-Liquid-Induced Transition from Coaxial Electrospray to Electrospinning of Low-Viscosity Poly(Lactide-Co-Glycolide) Sheath Solution. *Macromolecules* **2014**, 47, 7930-7938.
17. Wang, X.; Pellerin, C.; Bazuin, C. G. Enhancing the Electrospinnability of Low Molecular Weight Polymers Using Small Effective Cross-Linkers. *Macromolecules* **2016**, 49, 891-899.
18. Rayleigh, J. W. S. *Theory of Sound*; Macmilllan and Co.: New York, 1896.
19. Toimil-Molares, M. E.; Balogh, A. G.; Cornelius, T. W.; Neumann, R.; Trautmann, C. Fragmentation of Nanowires Driven by Rayleigh Instability. *Appl. Phys. Lett.* **2004**, 85, 5337-5339.
20. Dijksman, J. F.; Duineveld, P. C.; Hack, M. J. J.; Pierik, A.; Rensen, J.; Rubingh, J. E.; Schram, I.; Vernhout, M. M. Precision Ink Jet Printing of Polymer Light Emitting Displays. *J. Mater. Chem.* **2007**, 17, 511-522.
21. Grace, J. M.; Marijnissen, J. C. M. A Review of Liquid Atomization by Electrical Means. *J. Aerosol Sci.* **1994**, 25, 1005-1019.

22. Yurteri, C. U.; Hartman, R. P. A.; Marijnissen, J. C. M. Producing Pharmaceutical Particles Via Electrospraying with an Emphasis on Nano and Nano Structured Particles - a Review. *Kona Pow. Paricle J.* **2010**, 91-115.
23. Stachewicz, U.; Dijksman, J. F.; Yurteri, C. U.; Marijnissen, J. C. M. Volume of Liquid Deposited Per Single Event Electrospraying Controlled by Nozzle Front Surface Modification. *Microfluid. Nanofluid.* **2010**, 9, 635-644.
24. Stachewicz, U.; Yurteri, C. U.; Marijnissen, J. C. M.; Dijksman, J. F. Stability Regime of Pulse Frequency for Single Event Electrospraying. *Appl. Phys. Lett.* **2009**, 95.
25. Stachewicz, U.; Yurteri, C. U.; Dijksman, J. F.; Marijnissen, J. C. M. Single Event Electrospraying of Water. *J. Aerosol Sci.* **2010**, 41, 963-973.
26. Stachewicz, U.; Dijksman, J. F.; Yurteri, C. U.; Marijnissen, J. C. M. Experiments on Single Event Electrospraying. *Appl. Phys. Lett.* **2007**, 91.
27. Tjahjadi, M.; Ottino, J. M.; Stone, H. A. Estimating Interfacial-Tension Via Relaxation of Drop Shapes and Filament Breakup. *Aiche Journal* **1994**, 40, 385-394.
28. Stachewicz, U.; Bailey, R. J.; Wang, W.; Barber, A. H. Size Dependent Mechanical Properties of Electrospun Polymer Fibers from a Composite Structure. *Polymer* **2012**, 53, 5132-5137.
29. Arinstein, A.; Burman, M.; Gendelman, O.; Zussman, E. Effect of Supramolecular Structure on Polymer Nanofibre Elasticity. *Nat. Nanotechnol.* **2007**, 2, 59-62.
30. Zhang, Y.; Rutledge, G. C. Electrical Conductivity of Electrospun Polyaniline and Polyaniline-Blend Fibers and Mats. *Macromolecules* **2012**, 45, 4238-4246.
31. Richard-Lacroix, M.; Pellerin, C. Molecular Orientation in Electrospun Fibers: From Mats to Single Fibers. *Macromolecules* **2013**, 46, 9473-9493.
32. Diez, J. A.; Gonzalez, A. G.; Kondic, L. On the Breakup of Fluid Rivulets. *Phys. Fluids* **2009**, 21.
33. Owens, D. K.; Wendt, R. C. Estimation of the Surface Free Energy of Polymers. *J. Appl. Polym. Sci.* **1969**, 13, 1741-1747.
34. Goodwin, J. W.; Hughes, R. W. *Rheology for Chemists: An Introduction*; Royal Society of Chemistry: Cambridge, 2000.
35. Ansarifar, A.; Wang, L.; Ellis, R. J.; Haile-Meskel, Y. Using a Silanized Silica Nanofiller to Reduce Excessive Amount of Rubber Curatives in Styrene-Butadiene Rubber. *J. Appl. Polym. Sci.* **2011**, 119, 922-928.
36. Ismail, H.; Shaari, S. M.; Othman, N. The Effect of Chitosan Loading on the Curing Characteristics, Mechanical and Morphological Properties of Chitosan-Filled Natural Rubber (Nr), Epoxidised Natural Rubber (Enr) and Styrene-Butadiene Rubber (Sbr) Compounds. *Polym. Test.* **2011**, 30, 784-790.
37. Lodge, A. S. *Elastic Liquids: An Introductory Vector Treatment of Finite-Strain Polymer Rheology*; Academic Press: London, 1964.
38. Grant, R. P.; Middleman, S. Newtonian Jet Stability. *AICHE J.* **1966**, 12, 669-678.
39. Diez, J. A.; González, A. G.; Kondic, L. On the Breakup of Fluid Rivulets. *Physics of Fluids (1994-present)* **2009**, 21, 082105.
40. Brochard-Wyart, F.; Redon, C. Dynamics of Liquid Rim Instabilities. *Langmuir* **1992**, 8, 2324-2329.
41. Roy, R. V.; Schwartz, L. W. On the Stability of Liquid Ridges. *Journal of Fluid Mechanics* **1999**, 391, 293-318.
42. Stachewicz, U.; Li, S.; Bilotti, E.; Barber, A. H. Dependence of Surface Free Energy on Molecular Orientation in Polymer Films. *Appl. Phys. Lett.* **2012**, 100, 094104-4.
43. Maeda, K.; Bismarck, A.; Briscoe, B. Effect of Bulk Deformation on Rubber Adhesion. *Wear* **2007**, 263, 1016-1022.
44. Barber, A. H.; Cohen, S. R.; Wagner, H. D. Static and Dynamic Wetting Measurements of Single Carbon Nanotubes. *Phys. Rev. Lett.* **2004**, 92, 186103.

45. Barber, A. H.; Cohen, S. R.; Wagner, H. D. External and Internal Wetting of Carbon Nanotubes with Organic Liquids. *Phys. Rev. B* **2005**, 71, 115443.

TOC

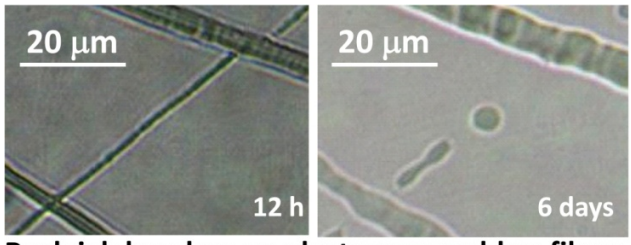

Rayleigh breakup on electrospun rubber fibers